IEEE Access
Multidisciplinary | Rapid Review | Open Access Journal

Date of publication xxxx 00, 0000, date of current version xxxx 00, 0000.

Digital Object Identifier 10.1109/ACCESS.2017.Doi Number

Metasurface-Inspired Flexible Wearable MIMO Antenna Array for Wireless Body Area Network Applications and Biomedical Telemetry Devices

Ayman A. Althuwayb[1], *Member IEEE*, Mohammad Alibakhshikenari[2], *Member IEEE*, Bal S. Virdee[3], *IEEE Senior Member*, Nasr Rashid[1], Khaled Kaaniche[1], Ahmed Ben Atitallah[1], Ammar Armghan[1], *IEEE Senior Member*, Osama I. Elhamrawy[1], Chan Hwang See[4], *IEEE Senior Member*, and Francisco Falcone[5,6], *IEEE Senior Member*

[1]Electrical Engineering Department, College of Engineering, Jouf University, Sakaka, Aljouf, 72388, Saudi Arabia
[2]Department of Signal Theory and Communications, Universidad Carlos III de Madrid, 28911 Leganés, Madrid, Spain
[3]Center for Communications Technology, London Metropolitan University, London N7 8 DB, U.K.
[4]School of Engineering and the Built Environment, Edinburgh Napier University, 10 Colinton Rd., Edinburgh, EH10 5DT, U.K.
[5]Department of Electric, Electronic and Communication Engineering and the Institute of Smart Cities, Public University of Navarre, 31006 Pamplona, Spain
[6]School of Engineering and Sciences, Tecnologico de Monterrey, Monterrey 64849, Mexico

Corresponding authors: Ayman A. Althuwayb (aaalthuwayb@ju.edu.sa), Mohammad Alibakhshikenari (mohammad.alibakhshikenari@uc3m.es) , Francisco Falcone (francisco.falcone@unavarra.es)

This work was funded by the Deanship of Scientific Research at Jouf University under Grant Number (DSR2022-RG-0110). Besides that, Dr. Mohammad Alibakhshikenari acknowledges support from the CONEX-Plus programme funded by Universidad Carlos III de Madrid and the European Union's Horizon 2020 research and innovation programme under the Marie Sklodowska-Curie grant agreement No. 801538. In addition, this work was supported by Ministerio de Ciencia, Innovación y Universidades, Gobierno de España (Agencia Estatal de Investigación, Fondo Europeo de Desarrollo Regional -FEDER-, Eu-ropean Union) under the research grant PID2021-127409OB-C31 CONDOR.

ABSTRACT This article presents a sub-6GHz ISM-band flexible wearable MIMO antenna array for wireless body area networks (WBANs) and biomedical telemetry devices. The array is based on metasurface inspired technology. The antenna array consists of 2×2 matrix of triangular-shaped radiation elements that were realized on 0.8 mm thick Rogers RT/duroid 5880 substrate. Radiation characteristics of the array are enhanced by isolating the surface current interaction between the individual radiators in the array. This is achieved by inserting an electromagnetic bandgap (EBG) decoupling structure between the radiating elements. The radiating elements were transformed into a metasurface by etching sub-wavelength slots inside them. The periodic arrangement of slots acts like resonant scatterers that manipulate the electromagnetic response of the surface. Results confirm that by employing the decoupling structure and sub-wavelength slots the isolation between the radiators is significantly improved (>34.8 dB). Moreover, there is an improvement in the array's fractional bandwidth, gain and the radiation efficiency. The optimized array design for operation over 5.0-6.6 GHz has an average gain and efficiency of 10 dBi and 83%, respectively. Results show that the array's performance is not greatly affected by a certain amount of bending. In fact, the antenna maintains a gain between 8.65-10.5 dBi and the efficiency between 77-83%. The proposed MIMO antenna array is relatively compact, can be easily fabricated on one side of a dielectric material, allows easy integration with RF circuitry, is robust, and maintains its characteristics with some bending. These features make it suitable for various wearable applications and biomedical telemetry devices.

INDEX TERMS On-body antennas, wearable antennas, flexible antennas, metasurface (MTS) antennas, electromagnetic bandgap (EBG) devices, biomedical telemetry devices, wireless body area network (WBAN), MIMO antenna array.

I. INTRODUCTION

The use of flexible wireless devices is rapidly growing, and this is mainly for health monitoring systems. This is a direct consequence of policy maker's decision to shorten the stay of patients in hospitals to cut healthcare costs. As a result, ambulatory health monitoring of patients has moved to the home. Furthermore, there is a growing trend of older citizens who do not want to live in an assisted living facility like care homes. This is because they cannot afford the exorbitant costs, or they prefer to be independent. As elderly people are living alone there is a need to monitor their wellbeing and safety. Hence, the need for wearable and implantable technologies has therefore become essential in the monitoring of critical physiological parameters of such people. The monitored data is either transmitted to a remote medical center or is used to direct the patient to take a specific action or is used to automatically perform a specific function based on what the sensors are reading. For example, if blood glucose is running high, insulin could be automatically administered [1][2].

Wearable devices for healthcare applications are expected to proliferate enormously and this is facilitated by Internet of Things (IoT) technology, which seamlessly connects via heterogeneous smart devices [3]. This is made possible with the ongoing deployment of 5G networks across many countries. 5G technology enables substantial improvement in wireless data rates, connectivity, bandwidth, coverage with the reduction in energy consumption and latency.

Wearable communications devices need to have a wide bandwidth to support Industrial Scientific Medical (ISM) and Wireless Local Area Network (WLAN) technologies. It is acknowledged that such devices cause higher levels of specific absorption rate (SAR) at the skin surface [4]. Based on the International Commission on Non-Ionizing Radiation Protection (ICNIRP) and the IEEE C95. 1-2019 standards, the SAR limit is set to 2 W/kg for the averaged over 10 g of tissue volume [5]. Wireless communications technology for wearable devices therefore requires antennas to have a smaller footprint to limit continuous radiation exposure on the body. However, the performance of standard antenna designs is compromised by miniaturization and interaction with the human body. The design of low-profile wearable antennas that possess multiband capability with a small footprint and whose radiation characteristics are not severely degraded by deformation of the antenna structure when worn on the body is a challenging proposition.

Microstrip patch antennas have been extensively used in the wearable antenna designs due to their planar structure [6][7]. Various antenna structures have been previously investigated considering the miniaturization and stable performance of the antenna on the human body. This includes the suitability of the planar inverted-F antenna (PIFA) reported in [8]. Unfortunately, this type of antenna suffers from a narrow impedance bandwidth due to its single resonance mode. Enhancing the impedance bandwidth of the PIFA to cover the whole 5 GHz WLAN band is a critical issue. Manipulating several resonance modes is one of the methods considered to widen the bandwidth. In [9], it is shown by loading shorting pins or vias is one technique to adjust the resonance frequency of PIFA. In [10], it is shown by etching slots in the patch antenna can achieve the same effect. Loading shorting pins and etching slots simultaneously to widen the desired impedance bandwidth of the PIFA have been studied by Liu et al. [11], [12]. In [11], the $TM_{0,1/2}$ and $TM_{0,3/2}$ modes of a PIFA were chosen to realize wideband performance however its fractional bandwidth is restricted to 11.8% by the high permittivity of the substrate. To further widen the operating bandwidth, an air layer was introduced as part of the substrate in [12], where the $TM_{0,1/2}$ and $TM_{2,1/2}$ modes are used to provide a fractional bandwidth of 15.3%. However, the mechanical stability of this type of antenna cannot be guaranteed in wearable applications. Antenna designs discussed above are complicated using shorting pins or vias which contribute towards the fabrication cost.

It has been demonstrated that multi-antenna technology like MIMO can increase the data rates, overcome multipath phenomena, and reduce power consumption [13]. The requirement for compactness of wearable devices using MIMO technology can however produce high interference among the radiating antenna elements. The electromagnetic interactions between the antenna elements due to surface currents can significantly degrade the performance of MIMO based wearable devices [14]. Therefore, to design a high-performance wearable multi-antenna system, the intra-system electromagnetic interference issues due to the mutual coupling between the radiating elements need to be mitigated. Hence, several approaches have been previously investigated to reduce mutual coupling in a multi-antenna system, by incorporating: (i) defected ground structure (DGS) [15]; (ii) electromagnetic bandgap (EBG) structure [16]; (iii) the parasitic element [17]; (iv) metamaterials-based isolator [18]; and (v) hybrid structure [19]. However, it is noted that in wearable applications, the multiple antennas are located on body, and design strategies for wearable antennas are quite different from the conventional ones. To meet the requirement of user's comfort it is important to select flexible materials for wearable applications. The challenge is to realize a wearable antenna whose performance is stable when subjected to a certain amount of deformation when worn on the body. The multi-antenna wearable antenna needs mutual coupling reduction approach that remains affective under severe bending conditions.

Numerous examples of wearables antennas have been investigated in the literature including MIMO antennas. For example, reported in [20] is a two-element dipole MIMO antenna implemented on textile for wearable applications. The antenna uses the ground plane as the main radiator, which is capacitively loaded by two strips along two edges to generate quasi-orthogonal radiation patterns. The isolation between the radiating elements is better than 12 dB over 2.4-3.0 GHz. The MIMO antenna in [21] is implemented on textile and exhibits dual-band response. The antenna is based on substrate integrated waveguide (SIW) technology and designed to resonate at 2.4 GHz. The second and third modes are excited and combined by placing a via within the SIW cavity to invoke resonance at 5 GHz. Isolation between the two radiators is better than 20 dB. By employing a pair of degenerated characteristic modes of a high-impedance surface circular loop antenna, the MIMO antenna in [22], which is designed to operate from 2.4-2.49 GHz, is shown to achieve port-to-port isolation better than 15 dB. Reported in [23] is a dual-port MIMO antenna that is constructed of Jeans material. It consists of standard rectangular patch antennas. To suppress mutual coupling between the antennas it employs two interconnected I-shaped stubs that are implemented on the ground plane and located between the two patches. The antenna operating over 2.4-8.0 GHz. With this technique the isolation achieved is better than 22 dB. A wideband (3.6-13 GHz) circularly polarized textile MIMO antenna for wearable applications is reported in [24]. The two radiating elements in the antenna consists of sickle-shaped radiators and a truncated ground plane with two L-shaped stubs located between the radiators. The isolation between the radiators is better than 18 dB. The MIMO antenna for wearable biotelemetric devices in [25] consists of four elements, which are placed orthogonally to the adjacent elements. The radiating elements are truncated corner patches with ground plane consisting of a hook-shaped open circuited stub. The antenna operates over 1.84-3.81 GHz and has isolation better than 20 dB.

More recently a wearable antenna 4×1 array is reported in [26]. The unit-cell of the array consists of a metasurface that is constructed from several square microstrip patches arranged in a cross configuration. Two opposite corners of the inner patched are slightly trimmed. The patch is excited from the bottom of the substrate with a single square patch on which a tilted slot is etched. The excitation patch is shielded with a ground-plane on bottom side of its substrate. The array operates across 4.51-6.43 GHz with a peak gain of 2.6 dBi. In [27] the 4×4 array is made fully using flexible textile materials using two felt substrate layers and conductive fabric as the conductive elements. The metasurface unit-cell consists of a square microstrip loop that encloses a square patch that is connected to the loop. The metasurface plane not only can generate positive resonances but also negative resonances due to its intrinsic properties. The array is excited from the bottom of the substrate with a slot feeding structure to induce anti-phase mode of the antenna. The array has a gain of -0.69 dBi at its lower resonance frequency of 2.45 GHz, and a gain of 7.4 dBi at 5.5 GHz.

In this paper a low-profile wearable MIMO antenna array design is presented that is constructed on a flexible substrate for wideband operation across 5.0-6.6 GHz. The isolation between the radiating elements in the array is significantly enhanced by mitigating the mutual coupling between the closely spaced radiating elements. This is achieved by employing EBG and metamaterial-inspired technologies. The EBG decoupling structure is inserted between the radiating elements and sub-wavelength slots are inserted in the patch antennas. Moreover, with this technique the effective aperture of the array is increased resulting in significantly improved bandwidth performance. Compared with other techniques reported in literature the proposed technique achieves isolation that is greater than 34.8 dB. Bending analysis of the array was also done to simulate complex bending condition scenarios encountered by on-body worn systems. The result of the bending analysis is shown to have minimal effect on the array's overall performance. These results confirm that the proposed antenna array is suitable for wireless body area networks that are used to monitor the health of patients.

II. The PROPOSED ANTENNA ARRAY

Reference antenna used in the study is a 2×2 array, shown in Fig.1(a). It consists of two pairs of inverted triangular shaped patches in close proximity. Triangular patch antenna was chosen in the array design because its sidelobes are suppressed to a greater extent than rectangular shaped patches [28]. The reverse side of the substrate is a ground plane. In the study the radiating elements in the prototype array were excited individually using microstrip feedlines. The ports of the array were combined to a common input using a power combiner and ensuring there is phase coherency at the ports.

The resonance frequency of the triangular patch antenna is determined by its dimensions and given by [29]

$$f_r = \frac{ck_{mn}}{2\pi\sqrt{\varepsilon_r}} \qquad (1)$$

Where c is the velocity of light, ε_r is the relative dielectric constant of the substrate, and k_{mn} is the wave number given by

$$k_{mn} = \frac{4\pi}{3a}\sqrt{m^2+mn+n^2} \qquad (2)$$

The lowest order resonance frequency is therefore given by

$$f_r = \frac{2c}{3a\sqrt{\varepsilon_r}} \qquad (3)$$

Where a is the length of the side of the triangular patch.

The dimensions of the patch radiators were calculated using standard Eqn.(3). The array was constructed on a Rogers RT/duroid 5880 with dielectric constant of (ε_r) of 2.2, loss-tangent ($\tan\delta$) of 0.0009, and thickness of 0.8 mm. The dimensions of the array are given in Table I and a picture of the fabricated array is shown in Fig. 1(b).

TABLE I
DIMENSIONS OF THE REFERENCE ANTENNA ARRAY

Thickness of Rogers RT/duroid 5880 substrate	0.8 mm
Height of equilateral triangular shaped patches	15.7 mm
Base length of equilateral triangular shaped patches	17.5 mm
Length of the feedline	3.1 mm
Width of the feedline	1.7 mm
Gap between the adjacent feedlines	24 mm
Gap between the opposite patches	4.6 mm
Overall dimensions of the antenna array	60×44×0.8 mm^3

The simulated and measured performance of the reference array are shown in Figs. 1(c)-(e). Fig.1(c) shows the measured impedance bandwidth of the reference array is 380 MHz for S_{11}≤-10 dB. The worst-case isolation measured over the operating frequency band of 5.66-6.04 GHz in Fig.1(c) between ports 1 & 2 is 13 dB at 6.0 GHz, ports 1 & 3 is 23 dB at 5.8 GHz, and ports 1 & 4 is 26 dB at 6.0 GHz. Fig.1(d) shows the minimum gain measured is 3.3 dBi at 5.66 GHz. From Fig.1(e) the worst-case efficiency measured is 54% at 5.66 GHz.

It's well known that mutual coupling between the adjacent radiators can adversely affect the performance of the antenna array. The coupling is predominately due to surface currents. To mitigate the unwanted coupling an electromagnetic bandgap (EBG) structure is inserted between the radiators as shown in Fig.2. EBG derive their name from an analogy to solid-state electronic bandgap structures. With the latter, there are certain energy bands that electrons can occupy and forbidden bands that cannot be occupied. With EBGs, the forbidden bands pertain to energy levels that photons cannot occupy. Hence, EM waves with a frequency inside the forbidden band cannot propagate through the EBG structure. Here we have implemented the EBG on a microstrip transmission-line by embedding resonant structures in the shape of triangular slots placed at regularly spaced distances.

The operating mechanism of this EBG structure can be explained by using an equivalent lumped element (LC) circuit model [28], where the capacitance is due to the slot gap and the inductance results from the current flowing in the microstrip-line. The resonance frequency of the circuit is given by $\omega_o = 1/\sqrt{LC}$. At low frequencies, the impedance is effectively inductive, and at high frequencies it is capacitive, and the structure supports transverse electric (TE) surface waves. Near the resonance frequency (ω_o), high impedance is obtained and the EBG does not support any surface waves, resulting in a frequency band gap blocking the flow of surface waves.

The bandgap property of the EBG structure in Fig.3(a) was verified with its dispersion diagram in Fig.3(b). The dispersion diagram was obtained using the Eigenmode Solver in CST Microwave Studio, which is a full-wave electromagnetic simulator. It shows the structure blocks surface current propagation between 5.1-6 GHz.

If there is sufficient gap between the radiating elements the inclusion of the EBG structure does not affect the overall size of the array. In fact, this technique can be retrofitted to existing arrays to improve the far-field radiation pattern of the array. The dimensions of the EBG structure are given in Table II. All other dimensions remain unchanged.

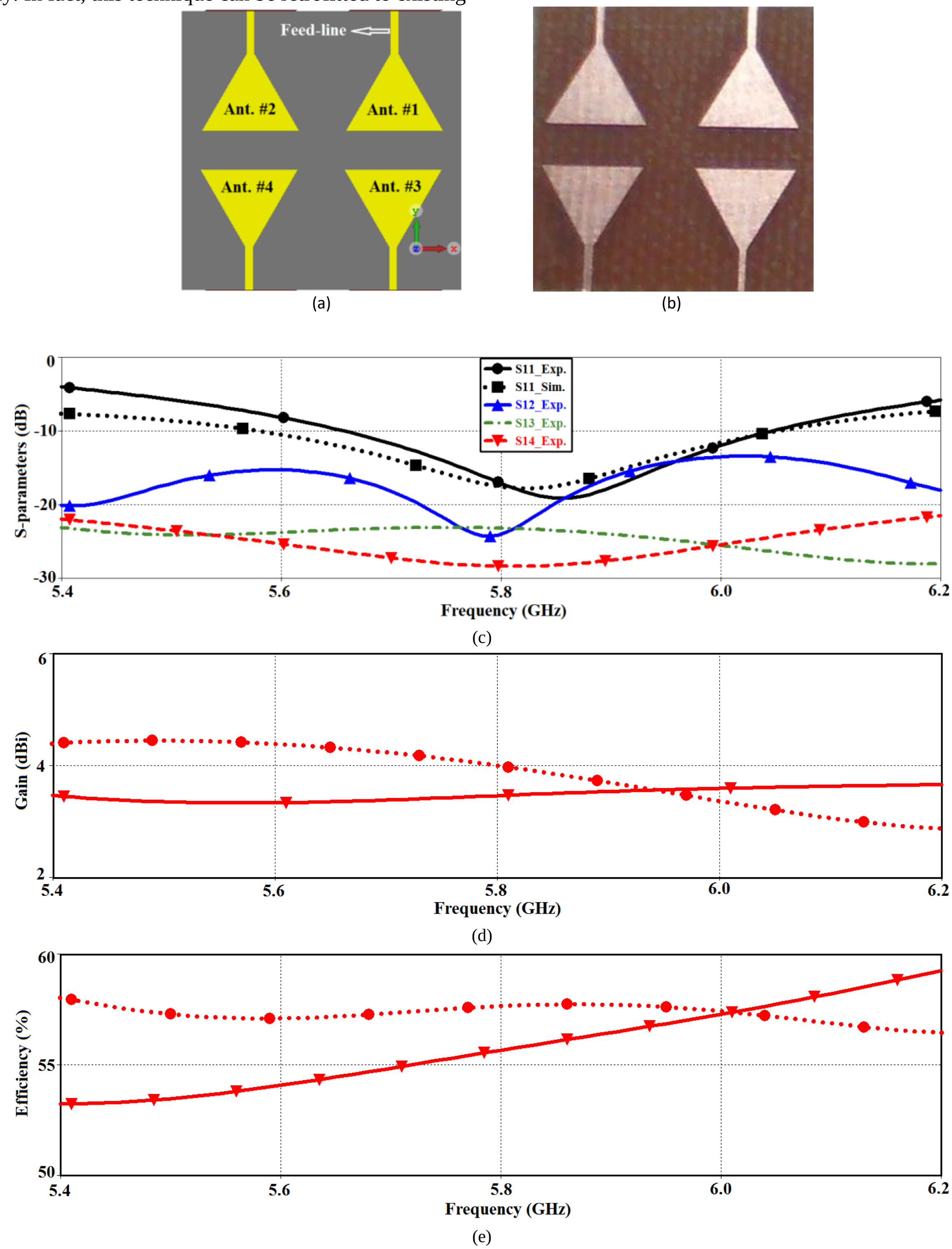

Fig.1. Reference 2×2 antenna array, (a) simulation layout, (b) photograph of the fabricated array (top side), (c) array's reflection-coefficient (S_{11}) & isolation between the patches (S_{12}, S_{13} & S_{14}), (d) antenna gain as a function of frequency, & (e) radiation efficiency as a function of frequency.

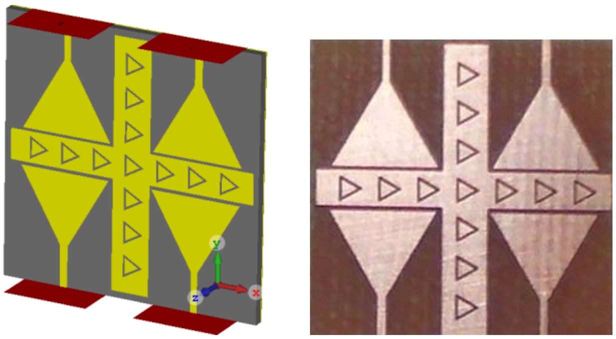

(a) (b)

Fig.2. (a) simulation layout of the 2×2 antenna array loaded with EBG decoupling structure, (b) photograph of the fabricated array (top side).

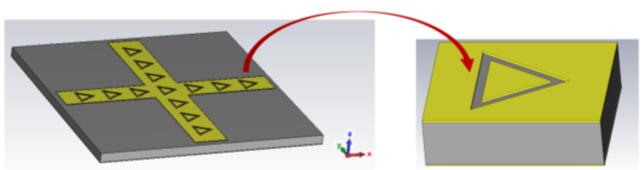

(a)

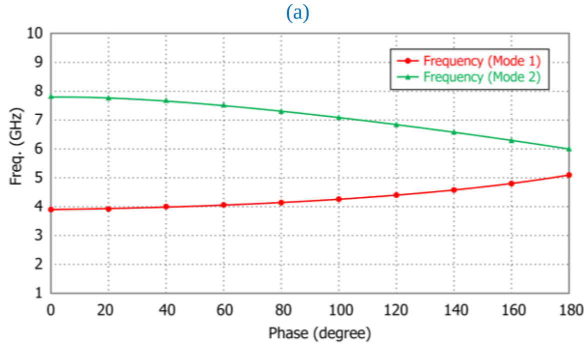

(b)

Fig.3 (a) The proposed EBG decoupling structure, and (b) dispersion diagram of the EBG structure obtained by CST Microwave Studio.

The simulated and measured performance of the antenna array without (WO) and with (W) the cross-shaped EBG decoupling structure are shown in Fig.4. The simulation was done using CST Microwave Studio. The measured results in Fig.4(a) show that without the decoupling structure the impedance bandwidth of the array is 380 MHz for S_{11}≤-10 dB. By inserting the decoupling structure, the bandwidth improves from 380 MHz to 810 MHz (5.32-6.13 GHz). Over the arrays operating frequency band, the measured isolation with the EBG structure between antennas 1 & 2 is >28 dB, between antennas 1 & 3 is >31 dB, and between antennas 1 & 4 >33 dB. Improvement in isolation between antennas 1 & 2 is 15 dB, between antennas 1 & 3 is 8 dB, and between antennas 1 & 4 is 7 dB. Fig.4(b) shows with the decoupling structure the measured gain varies between 6.8-7 dBi, and the radiation efficiency varies between 70-74%. These result show compared with the reference antenna the improvement in the gain and efficiency with the EBG structure are 3.5 dBi and 17%, respectively. These results are summarized in Tables III & IV.

Fig.5(a) shows the surface current density over the array without and with the EBG structure when just the top left antenna in the array is excited. From Fig.5(b) it can be observed the importance of including the EBG structure in significantly improving the isolation between the individual radiators.

TABLE II
DIMENSIONS OF THE ELECTROMAGNETIC BANDGAP (EBG) DECOUPLING STRUCTURE

Gap between the patch and decoupling structure	0.7 mm
Length of the decoupling structure	39.6 mm
Width of the decoupling structure	3.0 mm
Width of the triangular slots	0.35 mm
Length of sides of equilateral triangle slots	2.5 mm
Gap between the triangular slots	1.1 mm

TABLE III
COMPARISON OF THE PROPOSED ANTENNA ARRAY'S S-PARAMETERS WITHOUT AND WITH THE EBG DECOUPLING STRUCTURE.

Parameters (measured)	2×2 array without EBG decoupling structure	2×2 array with EBG decoupling structure	Improvement
Impedance bandwidth for $\|S_{11}\|$<-10 dB	380 MHz (5.66-6.04 GHz)	810 MHz (5.32-6.13 GHz)	113%
Isolation between antennas 1 & 2 ($\|S_{12}\|$) (dB)	>13	>28	15
Isolation between antennas 1 & 3 ($\|S_{13}\|$) (dB)	>23	>31	8
Isolation between antennas 1 & 4 ($\|S_{14}\|$) (dB)	>26	>33	7

TABLE IV
COMPARISON OF THE PROPOSED ANTENNA ARRAY'S GAIN AND EFFICIENCY PERFORMANCE WITHOUT AND WITH EBG DECOUPLING STRUCTURE.

Parameters (measured)	2×2 array without EBG decoupling structure	2×2 array with EBG decoupling structure	Improvement
Gain (dBi)	3.3	6.8	3.5
Radiation efficiency (%)	54	71	17

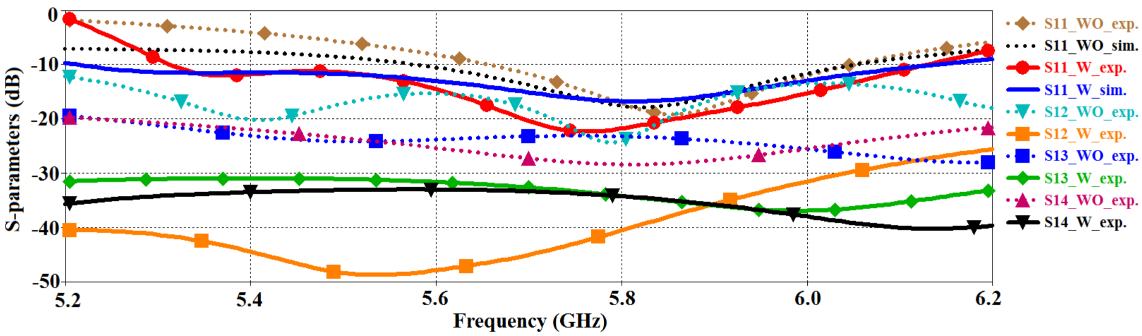

(a)

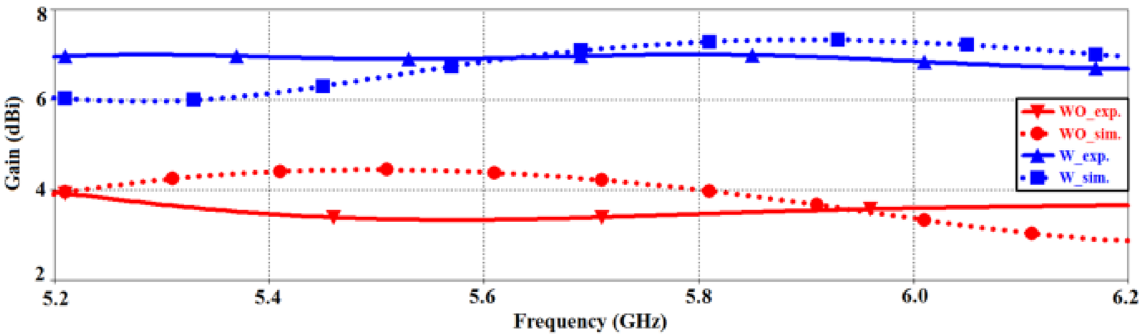

(b)

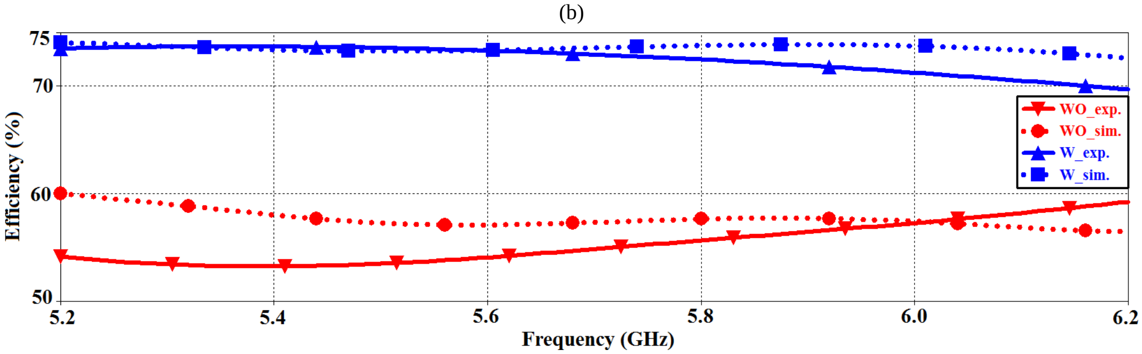

(c)

Fig.4. Antenna array's (a) reflection-coefficient (S_{11}) & isolation between the patches (S_{12}, S_{13} &S_{14}), (b) Gain as a function of frequency, & (c) Radiation efficiency as a function of frequency. Note, the abbreviations 'WO' stands for 'without' the EBG decoupling structure, and 'W' stands for 'with' the decoupling structure.

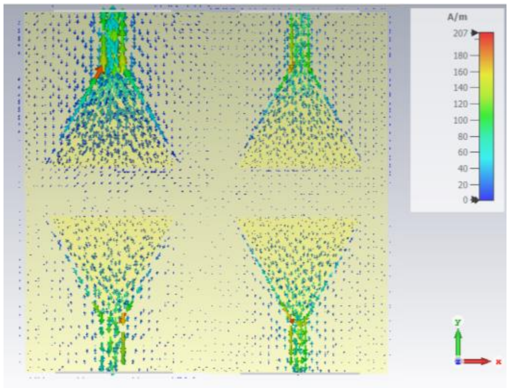

(a)

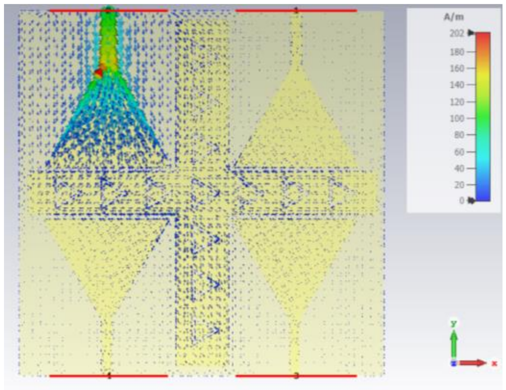

(b)

Fig.5. (a) Surface current density over the antenna array with no EBG structure when only the top left antenna is excited, and (b) surface current density over the antenna array with the proposed EBG structure.

The above results confirm the effectiveness of the proposed EBG decoupling technique in suppressing surface waves and thereby improving the isolation between the radiators as well as the gain and efficiency of the array.

To enhance the array's performance without increasing its physical dimensions the radiation elements of the array were transformed to metasurface. This was achieved by incorporating within the triangular patch an array of sub-wavelength resonant scatterers in the form of parallel slots of varying length which control the electromagnetic response of the surface [31]. The distribution of individual scatterers is crucial in determining the response of a patch surface. This configuration differentiates the metasurfaces from traditional frequency selective surfaces where the scatterers are of the order of the operating wavelength. The slots in the triangular shaped patches were etched as shown in Fig.6(a) & (b). The length of the slots is significantly smaller than the wavelength over which the array is operating. These slots are effectively resonant circuits that produce strong in-plane currents near resonance, which give rise to an effective magnetic surface current with a dominant dipolar response [32]. The dimensions of the slots are given in Table V. All other dimensions given in Table 1 remain unchanged.

TABLE V
DIMENSIONS OF THE SLOTS ETCHED INSIDE THE PATCHES.

Length of slot #1	1.0 mm
Length of slot #2	3.0 mm
Length of slot #3	5.6 mm
Length of slot #4	8.3 mm
Length of slot #5	10.7 mm
Width of slots	1.0 mm
Gap between slots	1.5 mm

Compared in Fig.6(c) & (d), respectively, are the measured reflection-coefficient and isolation responses of (i) the optimized antenna array loaded with EBG decoupling structure and slots, (ii) the reference array, and (iii) the array loaded with the EBG decoupling structure. It is observed that the impedance bandwidth of the optimized antenna array (EBG+slots) compared to the reference array improves by 1200 MHz (5.0-6.6 GHz). Moreover, there is improvement in the isolation. The isolation between antennas 1 & 2 is >34.8 dB, between antennas 1 & 3 is >35 dB, and between antennas 1 & 4 is >42 dB, i.e., the improvement is 21.8 dB, 12 dB, and 16 dB, respectively. These results are summarized in Tables VI. It is evident from these results that the slots have an effect of further reducing the surface waves and significantly enhancing the impedance bandwidth and isolation between the radiation elements.

Fig.7 shows the effect of the proposed approach on the radiation characteristics (gain and efficiency). Minimum gain and radiation efficiency measured in the case with EBG decoupling structure and slots are 8.9 dBi and 77%, respectively. Compared with the reference array the improvement in gain and efficiency are 5.6 dBi and 23%, respectively. The average measured gain and radiation efficiency across the frequency band (5-6.6 GHz) for the (i) reference array, (ii) array loaded by EBG decoupling structure, and (iii) optimized array loaded with EBG decoupling structure and slots are summarized in Table VII. The results reveal that the metamaterial slots effectively increase the aperture of the antenna array.

The simulated far-field radiation pattern of the reference antenna array and proposed 2×2 antenna array with the decoupling structure and metamaterial slots are shown in Fig.8. This figure shows there is marginal effect on the far-field by incorporating the decoupling structure and metamaterial slots. It also shows the array provides a wide coverage which is important for wearable applications. The actual radiation pattern of the reference and the proposed antenna arrays were measured in a controlled test environment inside an anechoic chamber. Pyramidal absorbers lined the chamber walls to absorb reflections and bring the electromagnetic noise level down well below the signals of interest. The measured radiation patterns of the reference antenna array in the *xz*- and *yz*-planes at the spot frequencies of 5 GHz, 5.7 GHz, and 6.6 GHz are shown in Fig.9. The results show the radiation patterns variation with frequency is not significant and the antenna predominantly radiates in the broadside direction. The measured radiation patterns of the proposed antenna array with the decoupling structure and metamaterial slots are shown in Fig.10. This figure also shows the radiation patterns variation with frequency is not significant however compared with the reference antenna array the backfire radiation is reduced by approximately 10 dB.

III. EVALUATION OF ANTENNA ARRAY FOR WEARABLE APPLICATIONS

Wearable antennas are increasingly used for on-body sensors to detect human motion and monitor human health parameters [33]. Wearable antennas need to be flexible to a certain degree and this should not impact significantly on its characteristics. Soon such antennas could be used in human machine interfacing, healthcare, robotics, and virtual reality. This section deals with the evaluating the compatibility of the proposed optimized antenna array for on-body worn scenarios. The versatility of the array is assessed under various deformation conditions and when located at different parts of the human body.

a. Bending scenarios

Under the on-body worn applications the antenna array is expected to bend. The impact on the antenna array's performance is evaluated when bend in the *xy*-plane. The antenna array is bend separately in the *xz*- and *yz*-planes. The bending radius was varied from 43 mm to 14 mm, as shown in Fig.11(a) & (b), and their corresponding reflection-coefficient, gain and radiation efficiency were measured. Fig.11(c) shows the impedance bandwidth is marginally reduced by 5.3% for bending radius of 14 mm & 17 mm in the *yz*-plane for S_{11}≤-10 dB. The impedance bandwidth for bending radii of 43–21 mm is unaffected. The reflection-coefficient results by bending the antenna array in the *xz*-plane in Fig.11(d) shows that the impedance bandwidth of bending radius 21 mm is reduced by 12.6%, 28 mm is reduced by 32%, and 43 mm is reduced by 5.3%. However, there is no impact on bending radii of 14 and 17 mm.

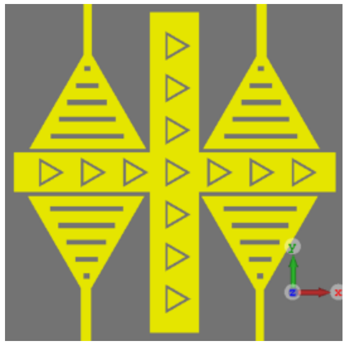

(a)

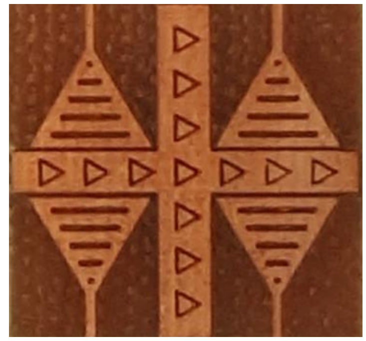

(b)

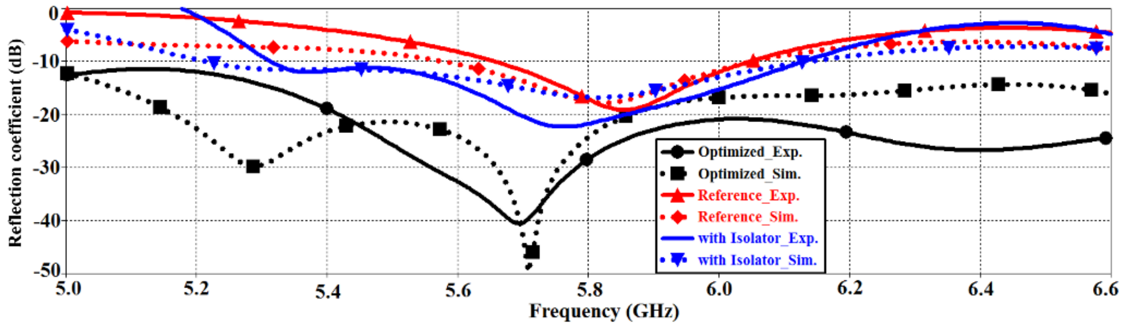

(c)

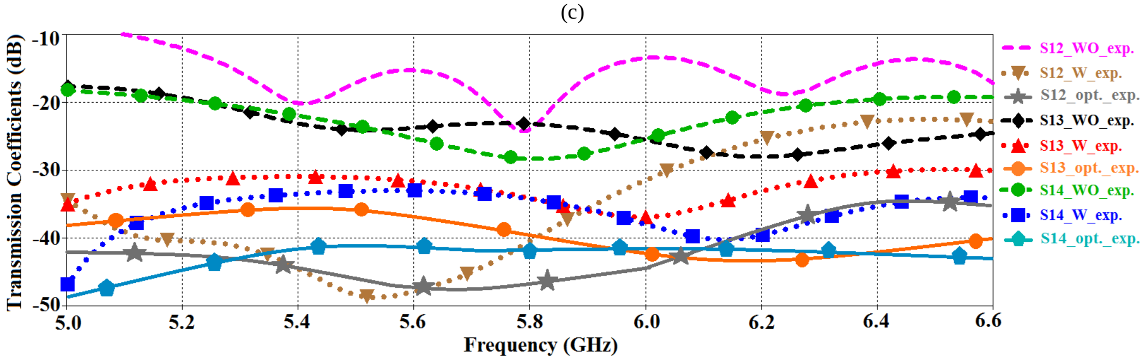

(d)

Fig.6. The proposed antenna array loaded with metasurface slots, (a) Simulation layout, (b) Photograph of the fabricated array (top side), (c) Array's reflection-coefficient (S_{11}) performance, and (d) Isolation response between the radiation patches (S_{12}, S_{13} &S_{14}). Abbreviation 'WO' and 'W' stand for 'without' and with 'W' the EBG and slots, respectively; and 'opt' is the optimized array with EBG and slots.

TABLE VI
S-PARAMETERS COMPARISON OF THE PROPOSED ANTENNA ARRAYS

Parameters (measured)	2×2 ref. array	2×2 array with EBG	2×2 array with EBG and slots (optimized)	Improvement c.f. ref. array
Impedance bandwidth for $\|S_{11}\|$<-10 dB	380 MHz (5.66-6.04 GHz)	810 MHz (5.32-6.13 GHz)	1600 MHz (5.0-6.6 GHz)	321%
Isolation between antennas 1 & 2 ($\|S_{12}\|$) (dB)	>13	>28	>34.8	21.8
Isolation between antennas 1 & 3 ($\|S_{13}\|$) (dB)	>23	>31	>35	12
Isolation between antennas 1 & 4 ($\|S_{14}\|$) (dB)	>26	>33	>42	16

TABLE VII
RADIATION PROPERTIES COMPARISON OF THE PROPOSED ARRAYS

Parameters (measured)	2×2 ref. array	2×2 array with EBG and without slots	2×2 array with EBG and without slots (optimized)	Improvement c.f. ref. array
Gain (dBi)	>3.3	>6.8	>8.9	5.6
Radiation efficiency (%)	>54	>71	>77	23

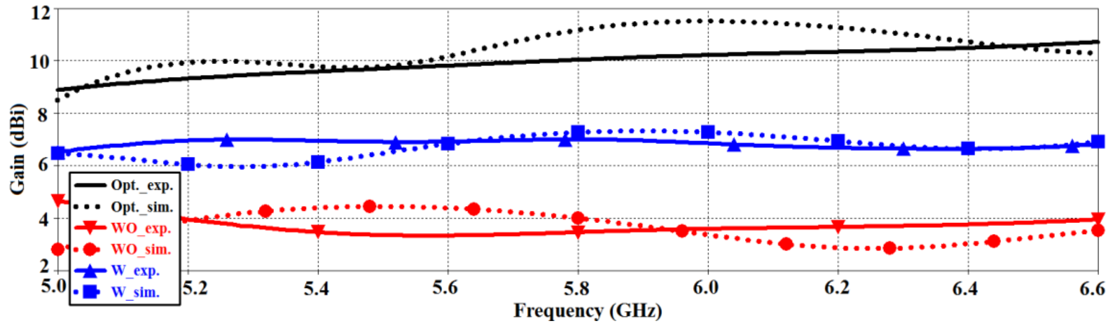

(a)

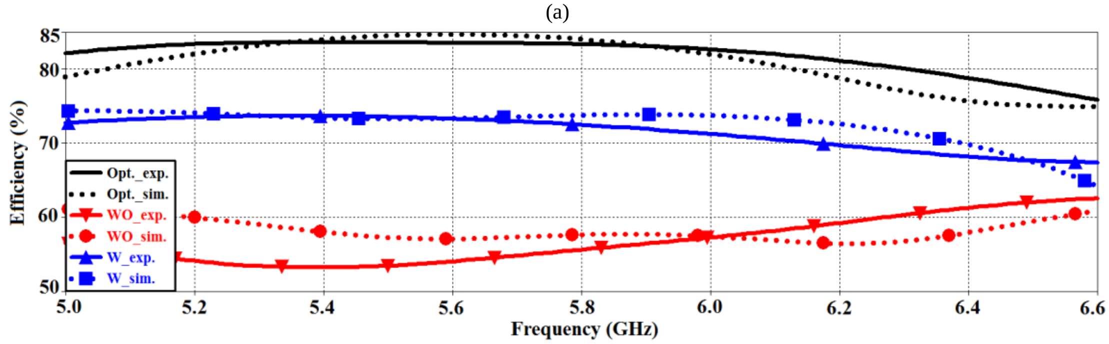

(b)

Fig.7. Radiation characteristics of the proposed antenna arrays, (a) Gain, and (b) Efficiency. Abbreviation 'WO' and 'W' stand for 'without' and with 'W' the EBG and slots, respectively; and 'opt' refers to the optimized array with EBG and slots.

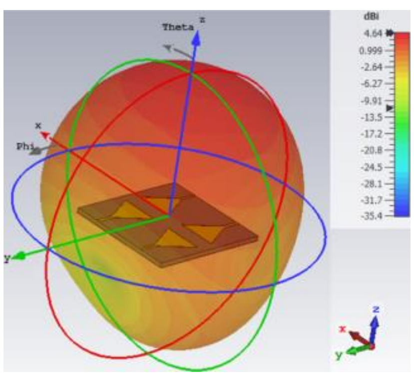

(a)

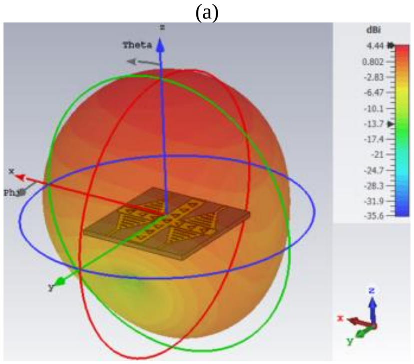

(b)

Fig.8. Simulated far-field radiation of the proposed antenna array (a) reference array, and (b) array with EBG decoupling structure and metasurface slots.

The gain response for various bending radii in the *yz*-plane between 5-6.6 GHz is shown in Fig.11(e). The gain for the largest bending radius of 43 mm varies from 8.4 dBi at 5 GHz to a peak of 11.5 dBi at 5.94 GHz. The gain for lowest bending radius of 14 mm varies from 8 dBi at 5.05 GHz to a peak of 9.8 dBi at 6 GHz. The gain in the *xz*-direction is shown in Fig.11(f). The gain for the largest bending radius of 43 mm varies from 9 dBi at 5 GHz to a peak of 11.2 dBi at 6.09 GHz. The gain for lowest bending radius of 14 mm varies from 8 dBi at 5.04 GHz to a peak of 9.8 dBi at 6.5 GHz. The relatively high gain is attributed to suppression of the mutual coupling effects between the antenna using EBG and ensuring phase coherency at the array ports.

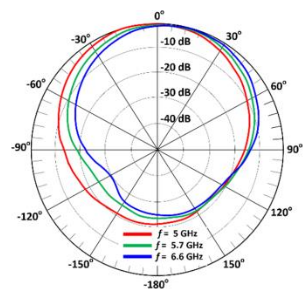

(a)

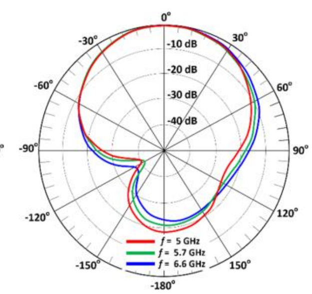

(b)

Fig.9. Measured radiation patterns of the reference antenna array, (a) *yz*-plane, and (b) *xz*-plane at 5 GHz, 5.7 GHz, and 6.6 GHz.

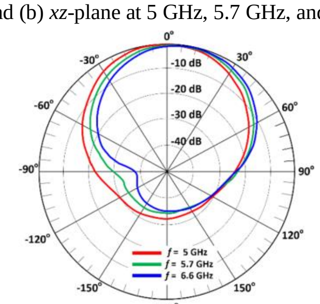

(a)

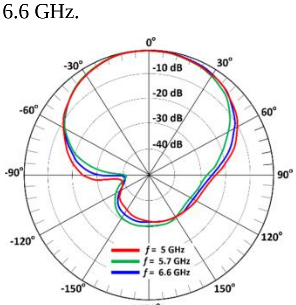

(b)

Fig.10. Measured radiation patterns the proposed antenna array with EBG decoupling structure and metasurface slots in (a) *yz*-plane, and (b) *xz*-plane at 5 GHz, 5.7 GHz, and 6.6 GHz.

The radiation efficiency in the *yz*-plane for various bending radii is shown in Fig.11(g). The results show for bending radius of 43 mm the efficiency varies from 83.5% at 5.4 GHz to 76% at 6.6 GHz. The efficiency for bending radius of 14 mm varies from 80.6% at 5.04 GHz to 75% at 6.5 GHz. By bending the antenna array in the *xz*-plane the radiation efficiency is correspondingly affected as shown in Fig.11(h). For bending radius of 43 mm the efficiency varies from 75.5% at 6.6 GHz to 84 at 5.68 GHz. The efficiency for bending radius of 14 mm varies from 75% at 6.56 GHz to 79.3% at 5.9 GHz. These results are summarized in Table VIII. The impact of the bending on the isolation are shown in Table IX. The total change in isolation measured by bending radius in the *yz*-plane is <1.2 dB. By bending radius in the *xz*-plane the change in isolation is <1.32 dB.

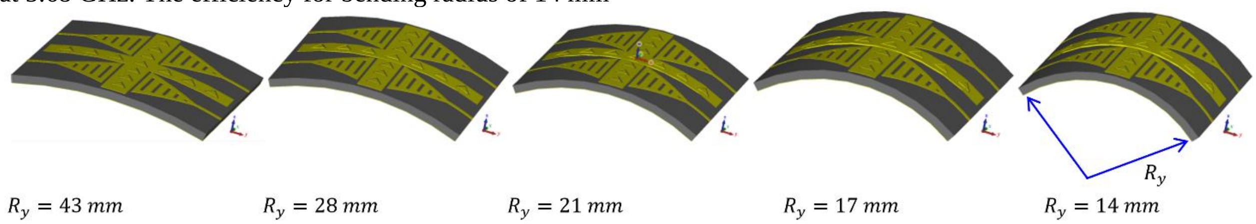

(a) *yz*-plane bending radius

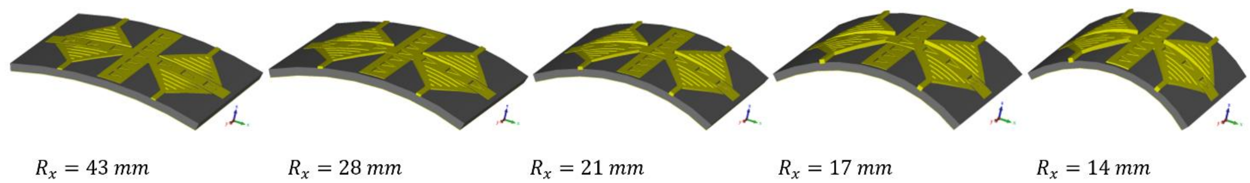

(b) *xz*-plane bending radius

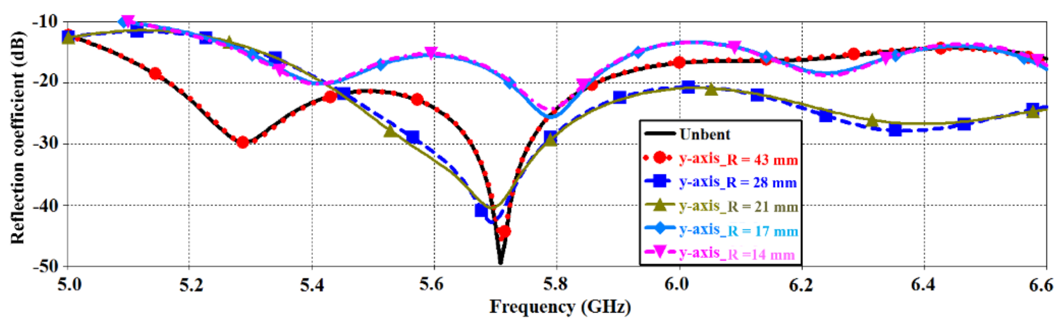

(c)

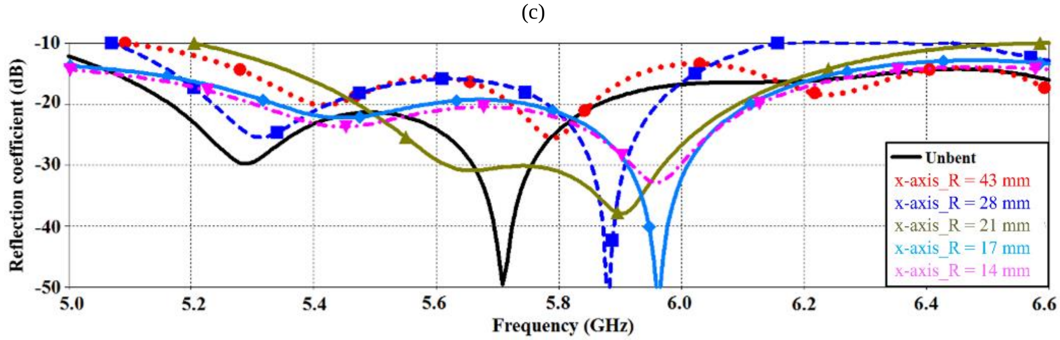

(d)

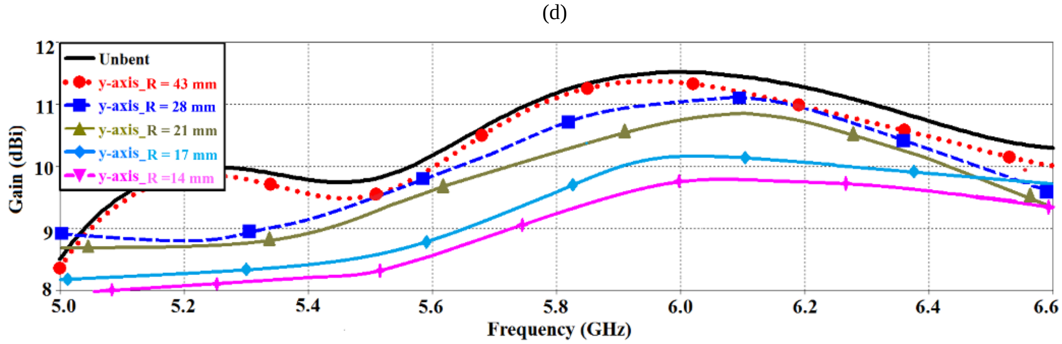

(e)

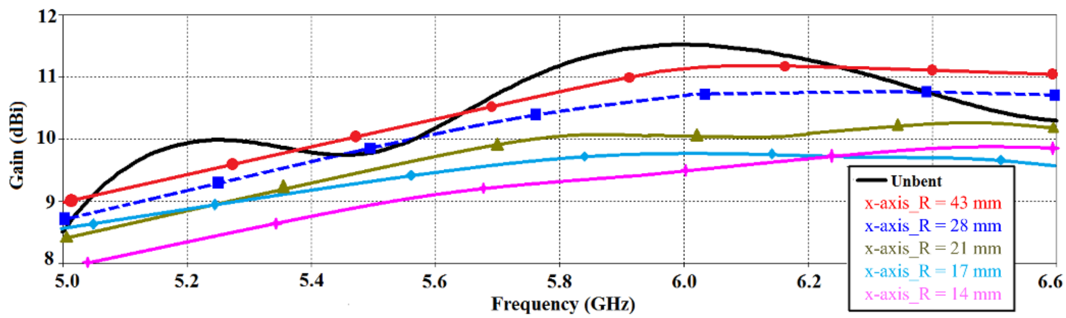

(f)

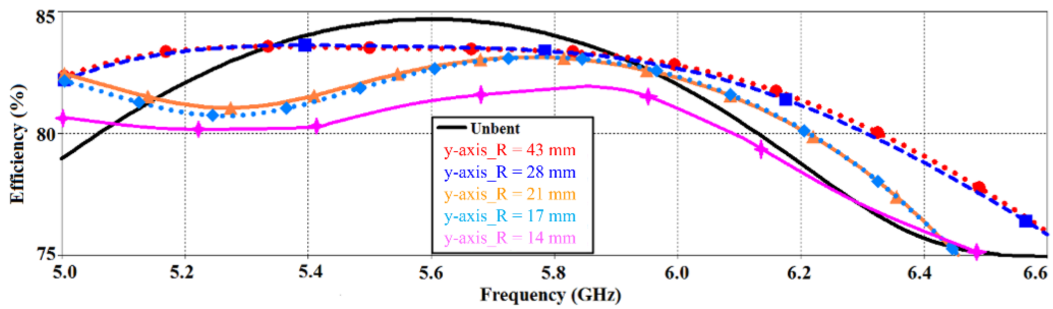

(g)

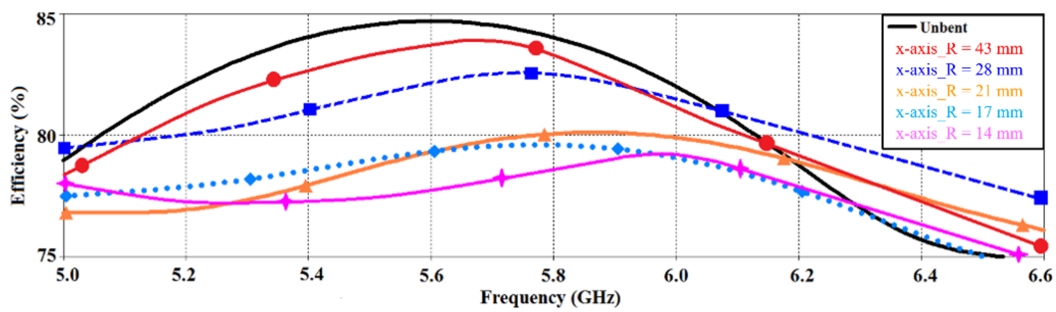

(h)

Fig.11. Deformation of the antenna array and its performance, (a) bending in the *yz*-plane, (b) bending in the *xz*-direction, (c) reflection-coefficients for various bend radii in the *yz*-plane, (d) reflection-coefficients for various bend radii in the *xz*-plane, (e) gain at various bend radii in the *yz*-plane, (f) gain at various bend radii in *xz*-plane, (g) radiation efficiency at various bend radii in the *yz*-plane, and (h) radiation efficiency at various bend radii in *xz*-plane.

TABLE VIII
COMPARISON OF THE ANTENNA ARRAY BENDING IN THE YZ- AND XZ-PLANES

BENDING IN THE YZ-PLANE

Parameters	Unbent	R_y = 43 mm	R_y = 28 mm	R_y = 21 mm	R_y = 17 mm	R_y = 14 mm
Frequency band (GHz)	5 - 6.6	5 - 6.6	5 - 6.6	5 - 6.6	5 - 6.6	5 - 6.6
Average gain (dBi)	10.5	10.4	10.3	10.2	9.5	9.4
Average efficiency (%)	83	82	84	82	81	81

BENDING IN THE XZ-PLANE

Parameters	Unbent	R_x = 43 mm	R_x = 28 mm	R_x = 21 mm	R_x = 17 mm	R_x = 14 mm
Frequency band (GHz)	5 - 6.6	5 - 6.6	5 - 6.6	5 - 6.6	5 - 6.6	5 - 6.6
Average gain (dBi)	10.5	10.4	10.3	9.8	9.3	9.4
Average efficiency (%)	83	82	82	78	77.5	77

TABLE IX
THE MEASURED ISOLATION PERFORMANCE OF THE PROPOSED ANTENNA ARRAY

BENDING IN THE YZ-PLANE OVER THE 5.0-6.6 GHZ BAND

Parameters	Unbent	R_y = 43 mm	R_y = 28 mm	R_y = 21 mm	R_y = 17 mm	R_y = 14 mm	Total change
Isolation between antennas 1 & 2 ($\|S_{12}\|$) dB	34.8	34.70	34.61	34.52	33.84	33.60	1.2

Isolation between antennas 1 & 3 ($\|S_{13}\|$) dB	35	34.90	34.82	34.73	34.1	33.75	1.15
Isolation between antennas 1 & 4 ($\|S_{14}\|$) dB	42	41.92	41.83	41.74	41.07	40.94	1.06

BENDING IN THE XZ-PLANE OVER THE 5.0-6.6 GHZ BAND

Parameters	Unbent	R_x = 43 mm	R_x = 28 mm	R_x = 21 mm	R_x = 17 mm	R_x = 14 mm	Total change
Isolation between antennas 1 & 2 ($\|S_{12}\|$) dB	34.8	34.65	34.54	34.43	33.75	33.53	1.27
Isolation between antennas 1 & 3 ($\|S_{13}\|$) dB	35	34.82	34.69	34.67	33.96	33.75	1.25
Isolation between antennas 1 & 4 ($\|S_{14}\|$) dB	42	41.89	41.76	41.68	41.01	40.68	1.32

b. On-Body Scenarios

In this section, the impact of human body loading on the antenna array's performance is evaluated using a realistic human body model called Hugo in CST Microwave Studio. Hugo allows accurate modeling of more than 30 human organs and tissues [34]. The array was loaded at different position on Hugo, as shown in Fig.12. This study complied with the maximum permissible specific absorption rate (SAR) for 10g of body tissue as defined in the IEEE/IEC 62704-1-2017 standard. Because of high permittivity and lossy nature of the human body we expect some variation in the results.

Table X shows the SAR values obtained from CST Microwave Studio according to the FCC standard. The proposed antenna array was place at two different locations on the body and excited with an input power of 0.2 W [35]. The input power is far more than will be used in reality. The FCC limit of 1.6 W/kg in Table X is not exceeded over the array's operating frequency range from 5-6 GHz. In practice, the maximum operating power used will be limited to 0 dBm (i.e., 1 mW).

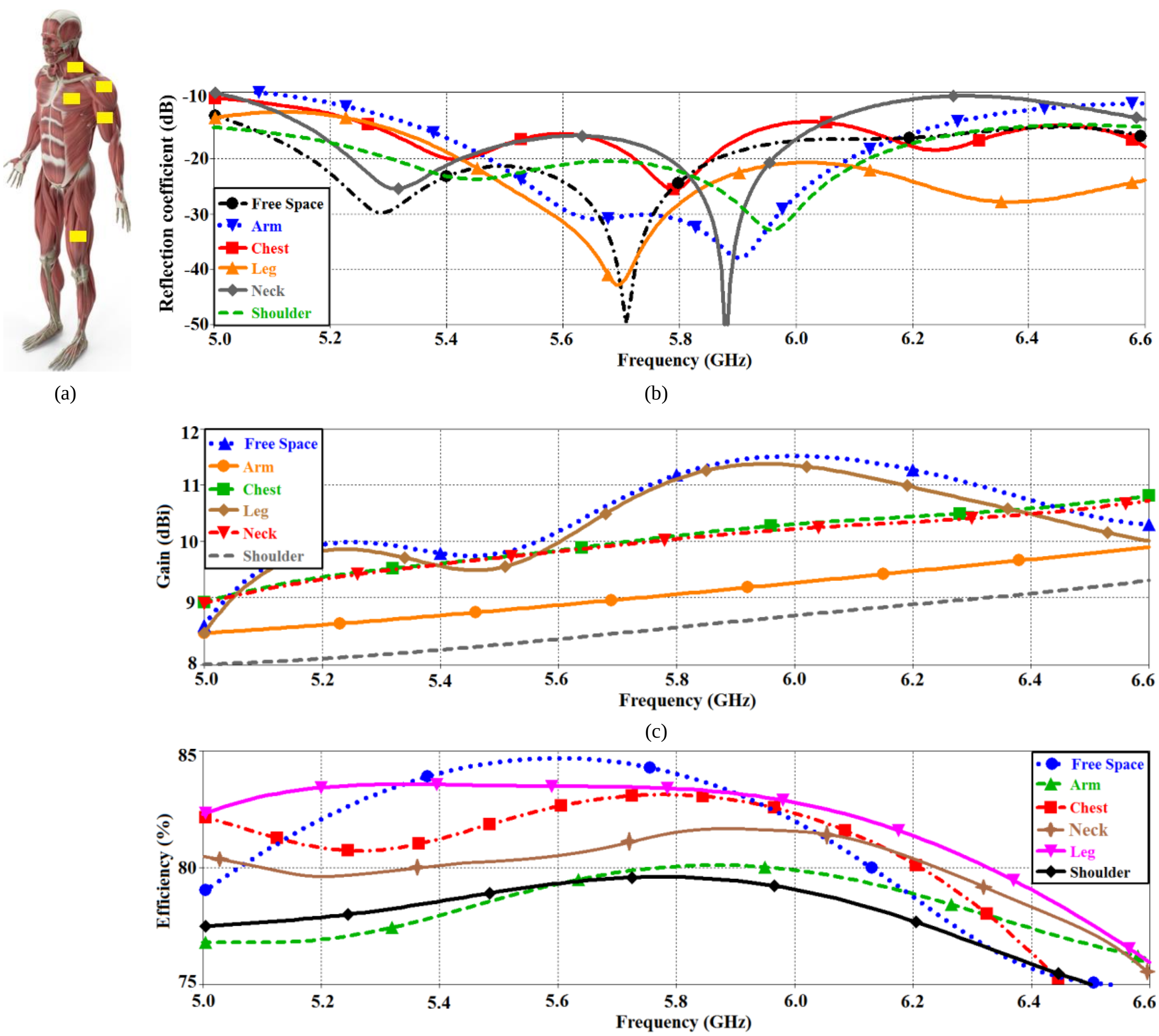

(d)

Fig.12. Evaluation of the antenna array's performance when mounted on the human body, (a) array placed at different locations on the human model, (b) on-body loading effect on the array's reflection-coefficient, (c) on-body loading effects on the array's radiation gain, and (d) on-body loading effect on the array's radiation efficiency.

TABLE X
SAR VALUE OF THE ANTENNA ARRAY

Freq.	Position	SAR (10g)
5 GHz	Neck	1.08 W/kg
	Chest	1.13 W/kg
	Shoulder	1.09 W/kg
	Arm	0.98 W/kg
	Thigh	1.12 W/kg
6 GHz	Neck	1.05 W/kg
	Chest	1.1 W/kg
	Shoulder	1.06 W/kg
	Arm	0.84 W/kg
	Thigh	1.07 W/kg

The measured reflection-coefficient response of the antenna array in free-space and when placed on the arm, chest, leg, neck and shoulder are shown in Fig.12. The impedance bandwidth of the array is unaffected however is marginally reduced by 4.6% for S_{11}≤-10 dB when placed on the arm. It is observed in Fig.12(b) that the resonant frequency of the array shifts when located at different positions on the body. The shift in the resonance frequency at the arm is 5.9 GHz, at the chest is 5.79 GHz, at the leg is 5.69 GHz, and at the shoulder is 5.97 GHz. The free-space gain in Fig.12(c) varies between 8.5-11.6 dBi. The gain varies almost linearly from 5-6.6 GHz for the case when mounted on the arm, chest, neck and shoulder. The gain varies between 8.5-9.9 dBi when the array is placed on the arm, between 9-10.9 dBi at the chest, between 8.8-11.4 dBi at the leg, between 9-10.8 dBi at the neck, and between 8-9.4 dBi at the shoulder. The effect on the array's radiation efficiency across 5-6.5 GHz is shown in Fig.12(d). The efficiency in free-space varies between 83-75%. When the array is placed on the arm the efficiency changes between 77-75.8%, on the chest it changes between 83-75%, on the neck it changes between 81.6-75.6%, on the leg it changes between 83.6-75.8%, and on the shoulder it changes between 79.6-75%. These results are summarized in Table XI. The results in the table show that there is marginal impact on the performance of the proposed array when placed on the human body. This makes the array suitable for biosensors and wireless body area network applications.

Envelope correlation coefficient (*ECC*) indicates the correlation between the radiating antenna elements. *ECC* can be determined from S-parameters measurements using [36]

$$ECC = \frac{|S_{11}^* S_{12} + S_{22}^* S_{21}|^2}{[1-(|S_{11}|^2+|S_{21}|^2)][1-(|S_{22}|^2+|S_{12}|^2)]} \quad (1)$$

The corresponding diversity gain (*DG*) is calculated using [36]

$$DG = 10\sqrt{1-ECC} \quad (2)$$

Ideally the magnitude of *ECC* should be zero, however, in practical applications an *ECC* <0.5 is acceptable. Fig.13 show how the measured *ECC* and *DG* vary across the proposed array's frequency range. The correlation is <0.05 between the antennas in the array, and *DG* is >9.7 dB. This confirms an excellent diversity performance by the proposed array which makes it suitable for high data rate transmission.

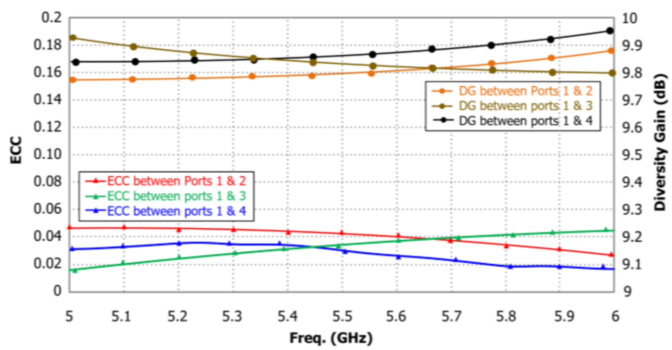

Fig.13. The measured envelop correlation coefficient (ECC) and diversity gain (DG) of the proposed 2×2 element antenna array.

TABLE XI
ON-BODY LOADING IMPACT ON THE ARRAY'S PERFORMANCE

Parameter (measured)	Free space	Leg	Chest	Neck	Arm	Shoulder
Resonance frequency (GHz)	5.71	5.69	5.79	5.87	5.9	5.97
Average gain (dBi)	10.5	10.35	9.8	9.7	9.15	8.64
Average efficiency (%)	83	82	81	80	78	77

c. *Total Active Reflection Coefficient (TARC)*

The ratio of the square root of total reflected power divided by the square root of total incident power defines TARC [55]. The TARC at *N* port antenna is given by

$$\Gamma_a^t = \sqrt{\sum_{i=1}^{N} |b_i|^2} \Big/ \sqrt{\sum_{i=1}^{N} |a_i|^2} \quad (4)$$

Where a_i is incident wave and b_i is the reflected wave.

In the case of 2×2 antenna array, the scattering matrix can be described as

$$\begin{pmatrix} b_1 \\ b_2 \end{pmatrix} = \begin{pmatrix} s_{11} & s_{12} \\ s_{21} & s_{22} \end{pmatrix} \begin{pmatrix} a_1 \\ a_2 \end{pmatrix} \quad (5)$$

Where $b_1 = a_1(s_{11} + s_{12}e^{i\theta})$ (6)

$b_2 = a_1(s_{21} + s_{22}e^{i\theta})$ (7)

As MIMO channels are assumed as Gaussian and multipath spread in the propagation medium it is therefore assumed the reflected wave will be unity magnitude but randomly phased with independent and identically distributed Gaussian random variable [55]. Since sum or subtraction of independent Gaussian random variables is also Gaussian, TARC is represented by

$$\Gamma_a^t = \sqrt{(|(s_{11} + s_{12}e^{j\theta})|^2 + |(s_{21} + s_{22}e^{j\theta})|^2)}/\sqrt{2} \quad (8)$$

Eqn.(8) was used to calculate the TARC for the proposed 2×2 antenna array, which is shown in Fig.14. The figure also shows the TARC calculated from the measurements at various spot frequencies. The TARC response is identical for excitation at the different ports, which is unsurprising as the array is a symmetrical structure. It is evident that the TARC retains the original behavior of a single antenna characteristic however the bandwidth and return-loss are changed because TARC contains the effect of mutual coupling and the phase of incident signal.

IV. COMPARISON WITH OTHER WEARABLE ANTENNA

The salient features of the proposed antenna array are compared in Table XII with representative wearable antennas reported in the literature. The comparison parameters include dimensions, frequency of operation, fractional bandwidth, inter-antenna isolation, gain and radiation efficiency. The comparison with MIMO antenna arrays of various matrix size including 4×4 shows that the proposed array has the highest isolation greater than 34.8 dB, gain of 9.50 dBi and radiation of 80%. Comparison with the other 4-port arrays shows that the proposed 4-port array has a substantially higher gain performance. The size of the proposed array is comparable to the 4-port array in [25] and significantly smaller than the 4-port array reported in [26]. However, the 4-port MIMO array reported in [25] has a much larger fractional bandwidth of 91.66%. This demonstrates the proposed array is viable for many wearable applications and is a key component for leveraging the 5G technology in realizing future wireless solutions.

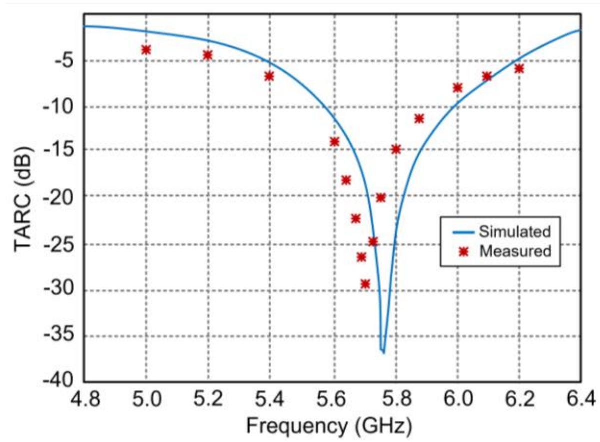

Fig.14. The simulated and measured TARC of the proposed 2×2 element antenna array.

TABLE XII
COMPARISON OF FLEXIBLE ANTENNAS REPORTED IN LITERATURE

Ref.	Design Technique	Material permittivity (ε_r)	Dimensions (mm^3)	On-body Frequency Range (GHz)	On-body Fractional Bandwidth (%)	Antenna type / On-body Average Isolation (dB)	On-body Average Gain (dBi)	On-body Average Efficiency (%)
[37]	EBG and frequency selective surface	Textile (1.7)	60×60×2.4	2.30 – 2.50	8.30	Single / –	6.55	–
[38]	EBG	Wool felt (1.2)	81×81×4	2.28 – 2.65	14.70	Single / –	7.30	70
[39]	Artificial magnetic conductor (AMC)	Pellon fabric (1.09)	102×68×3.6	4.30 – 5.90	34.00	Single / –	6.12	–
[40]	Fractal antenna with defected ground	RT/duroid 5880 (2.2)	39×39×0.503	2.36 – 2.55	7.75	Single / –	2.06	75
[41]	Metamaterial and split ring resonator	FR4 (4.3)	8.14×8.14×1.6	2.36 – 2.47	4.50	Single / –	-8.00	–
[42]	Slot elements & floating ground	Felt (1.36)	15×17×1	5.57 – 5.89	5.50	Single / –	4.85	48
[43]	EBG	FR4 (4.4)	120×120×2.2	2.40 – 2.50 5.15 – 5.825	4.0 12.3	Single / –	7.60	–
[44]	Square slotted EBG	Textile (1.7)	50×50×1	1.78 – 1.98 2.38 – 2.505	10.92 5.08	Single / –	–	–
[45]	Magnetic wall & open-ended quarter wavelength slot	Rogers Duroid 5870 (2.33)	42×30×1.58	2.425 – 2.455 5.731 – 5.845	1.22 1.96	Single / –	2.13 5.16	60 76
[46]	Half-diamond shaped half-mode SIW	Rubber foam (1.495)	64.6×61.7×3.94	2.40 – 2.51 5.70 – 5.87	4.48 2.93	Single / –	4.10 5.80	72.8 85.6
[47]	Quarter-Mode SIW	Textile (-)	64×64×3.7	2.39 – 2.51	4.90	Single / –	4.20	81
[48]	Artificial magnetic conductor (AMC)	Textile (-)	60×45×1 62×50×1	2.20 – 2.75 2.30 – 2.53	22.22 9.52	Single / –	5.0 6.0	–

[49]	Metasurface with Anisotropic ground	Elastomer (2.67)	50×50×5.5	2.37 – 2.64	15.9	Single / –	5.2	79
[50]	Slotted Cross with AMC ground plane	Polyimide (3.5)	65.7×65.7×1.5	2.20 – 2.75	22.22	Single / –	4.8	–
[51]	Metasurface	Polyimide (3.5)	30×25×0.085	2.32 – 2.45 5.37 – 5.71	5.45 6.13	Single / –	5.2 7.7	61.3 67.2
[52]	EBG backed planar monopole structure	RT/duroid 5880 (2.2)	68×38×1.57	2.40 – 2.52	4.87	Single / –	6.88	76
[53]	Truncated metasurface	-	62×42×4	2.32 – 2.46	5.85	Single / –	6.20	–
[54]	AMC	Textile & felt (1.2)	100×100×1.5	2.30 – 2.70 5.20 – 5.80	16.0 10.90	Single / –	2.50 4.00	40 40
[20]	Dipole	Textile (-)	38.1×38.1×2	2.4 – 3.0	20	2-port MIMO / 12	1.67	27
[21]	SIW	Textile & felt (1.3)	92.3×101.9×3	2.36 – 2.52, 5.18 – 5.86	6.55 12.31	2-port MIMO / 20	–	–
[22]	Circular high impedance surface	FR4 (4.4)	45.8×45.8×3.2	2.40 – 2.49	3.68	2-port MIMO / 15	4.2	63
[23]	Double 'I' shaped ground stubs	Textile (1.6)	40×70×1	2.4 – 8.0	107.69	2-port MIMO / 22	3	–
[24]	Sickle-shaped radiator	Textile (-)	32.5×42×1	3.6 – 13.0	113.25	2-port MIMO / 18	3	-
[25]	Modified square patch	FR4 (4.4)	40×40×1.6	1.84 – 3.81	91.66	4-port MIMO / 20	2	-
[26]	Wearable conformal antenna array	Textile & felt (-)	321×61×4	4.51 – 6.43	35.1	4-port MIMO / -	2.6	50
[27]	Wearable textile metasurface array	Textile & felt (1.3)	44.1×44.1×5	2.45 5.50	10.2 22.5	Single / -	-0.69 7.40	18 40
This work	**EBG & MTS**	**RT/duroid 5880 (2.2)**	**60×44×0.8**	**5.00 – 6.60**	**27.58**	**4-port MIMO / >34.8**	**9.50**	**80**

V. CONCLUSION

The results of a novel flexible wearable MIMO antenna design presented here has very high inter-antenna isolation of 34.8 dB compared to other antennas reported in literature. The antenna also exhibits desirable properties of wideband performance of gain of 9.50 dBi and radiation efficiency of 80%. The design of the antenna array combines electromagnetic bandgap and metasurface-inspired technologies. It is shown that unwanted surface waves on the planar array are significantly suppressed with the inclusion of an EBG decoupling structure placed between the radiating elements, and by inserting sub-wavelength slots in the patches. By doing this the surface waves are mitigated, and the effective aperture of the antenna is shown to enhance. This technique has no implications on the overall footprint of the array. Measured results confirm that the antenna's performance is marginally affected when it is bent in the *xz*- and *yz*-planes. It is also shown that the FCC limit of 1.6 W/kg is not exceeded over the array's operating frequency band. The results presented here demonstrate the proposed MIMO antenna is highly suitable for wearable systems including biomedical applications.

REFERENCES

[1] S. Majumder, T. Mondal, and M. J. Deen, "Wearable sensors for remote health monitoring," Sensors, vol. 17, issue 130, 2017, pp.1-45.

[2] Q. Liu, K. G. Mkongwa, C. Zhang, "Performance issues in wireless body area networks for the healthcare application: a survey and future prospects," Springer Nature Applied Sciences, 3;155, 2021, pp.1-19.

[3] H. Ullah, N. G. Nair, A. Moore, C. Nugent, P. Muschamp, M. Cuevas, "5G Communication: an overview of vehicle-to-everything, drones, and healthcare use-cases," IEEE Access, vol. 7, 2019, pp.37251-37268.

[4] S. Kim, Y. Sharif, I. Nasim, "Human Electromagnetic Field Exposure in Wearable Communications: A Review," Signal Processing, 2019, pp.1-13. arXiv:1912.05282.

[5] International Commission on Non-Ionizing Radiation Protection (ICNIRP). Guidelines for limiting exposure to electromagnetic fields (100 kHz to 300 GHz). Health Phys. 118, 2020, pp. 483–524.

[6] Z. G. Liu and Y. X. Guo, "Dual band low profile antenna for body centric communications," IEEE Trans. Antennas Propag., vol. 61, no. 4, Apr. 2013, pp. 2282–2285.

[7] T. T. Le and T.-Y. Yun, "Miniaturization of a dual-band wearable antenna for WBAN applications," IEEE Antennas and Wireless Propagation Letters, vol. 19, no. 8, August 2020, pp. 1452-1456.

[8] W. E. Hajj, C. Person, and J. Wiart, "A novel investigation of a broadband integrated inverted-F antenna design; application for wearable antenna," IEEE Trans. Antennas Propag., vol. 62, no. 7, Jul. 2014, pp. 3843–3846.

[9] N.-W. Liu, L. Zhu, W.-W. Choi, and X. Zhang, "A low-profile aperturecoupled microstrip antenna with enhanced bandwidth under dual resonance," IEEE Trans. Antennas Propag., vol. 65, no. 3, Mar. 2017, pp. 1055–1062.

[10] H. Wong, K. K. So, and X. Gao, "Bandwidth enhancement of a monopolar patch antenna with V-shaped slot for car-to-car and WLAN communications," IEEE Trans. Veh. Technol., vol. 65, no. 3, Mar. 2016, pp. 1130–1136.

[11] N.-W. Liu, L. Zhu, W.-W. Choi, and X. Zhang, "Wideband shorted patch antenna under radiation of dual-resonant modes," IEEE Trans. Antennas Propag., vol. 65, no. 6, Jun. 2017, pp. 2789–2796.

[12] N.-W. Liu, L. Zhu, and W.-W. Choi, "A low-profile wide-bandwidth planar inverted-F antenna under dual resonances: Principle and design approach," IEEE Trans. Antennas Propag., vol. 65, no. 10, Oct. 2017, pp. 5019–5025.

[13] D. Gesbert, M. Shafi, D. S. Shiu, P. J. Smith, and A. Naguib, "From theory to practice: An overview of MIMO space-time coded wireless systems," IEEE J. Sel. Areas Commun., vol. 21, no. 3, Apr. 2013, pp. 281–302.

[14] R. Janaswamy, "Effect of element mutual coupling on the capacity of fixed length linear arrays," IEEE Antennas Wireless Propag. Lett., vol. 1, 2002, pp. 157–160.

[15] R. Anitha, V. Sarin, P. Mohanan, and K. Vasudevan, “Enhanced isolation with defected ground structure in MIMO antenna,” Electron. Lett., vol. 50, no. 24, 2014, pp. 1784–1786.
[16] H. H. Park, “Reduction of electromagnetic noise coupling to antennas in metal-framed smartphones using ferrite sheets and multi-via EBG structures,” IEEE Trans. Electromagn. Compat., vol. 60, no. 2, Apr. 2018, pp. 394–401.
[17] S. Farsi, H. Aliakbarian, D. Schreurs, B. Nauwelaers, and G. A. E. Vandenbosch, “Mutual coupling reduction between planar antennas by using a simple microstrip U-section,” IEEE Antennas Wireless Propag. Lett., vol. 11, 2012, pp. 1501–1503.
[18] C.-C. Hsu, K.-H. Lin, and H.-L. Su, “Implementation of broadband isolator using metamaterial-inspired resonators and a T-shaped branch for MIMO antennas,” IEEE Trans. Antennas Propag., vol. 59, no. 10, Oct. 2011, pp. 3936–3939.
[19] A. C. Durgun, C. A. Balanis, C. R. Birtcher, H. Huang, and H. Yu, “High-impedance surfaces with periodically perforated ground planes,” IEEE Trans. Antennas Propag., vol. 62, no. 9, Sep. 2014, pp. 4510–4517.
[20] H. Li, S. Sun, B. Wang and F. Wu, “Design of compact single-layer textile MIMO antenna for wearable applications,” IEEE Transactions on Antennas and Propagation, vol. 66, no. 6, pp. 3136-3141, June 2018.
[21] S. Yan, P. J. Soh and G. A. E. Vandenbosch, “Dual-band textile MIMO antenna based on substrate-integrated waveguide (SIW) technology,” IEEE Transactions on Antennas and Propagation, vol. 63, no. 11, pp. 4640-4647, Nov. 2015.
[22] D. Wen, Y. Hao, M. O. Munoz, H. Wang and H. Zhou, “A compact and low-profile MIMO antenna using a miniature circular high-impedance surface for wearable applications,” IEEE Transactions on Antennas and Propagation, vol. 66, no. 1, pp. 96-104, Jan. 2018.
[23] A.K. Biswas, and U. Chakraborty, “A compact wide band textile MIMO antenna with very low mutual coupling for wearable applications,” Int. Journal of RF and Microwave Computer-Aided Engineering, vol. 29, issue 8, pp. 1-11, August 2019.
[24] S. Kumar et al., “Wideband circularly polarized textile MIMO antenna for wearable applications,” IEEE Access, vol. 9, pp. 108601-108613, 2021.
[25] A. Iqbal, et al., “Wideband circularly polarized MIMO antenna for high data wearable biotelemetric devices,” IEEE Access, vol. 8, pp. 17935-17944, 2020.
[26] H. Yang, X. Liu, and Y. Fan, “Design of broadband circularly polarized all-textile antenna and its conformal array for wearable devices,” IEEE Trans. Antennas Propag., vol. 70, no. 1, 209–220, Jan. 2022.
[27] K. Zhang, P.J. Soh, and S. Yan, “Design of a compact dual-band textile antenna based on metasurface,” IEEE Transactions on Biomedical Circuits and Systems, vol. 16, no. 2, pp. 211-221, April 2022.
[28] Y. S. H. Khraisat, M. M. Olaimat, “Comparison between rectangular and triangular patch antennas array,” 19th International Conference on Telecommunications (ICT), 2012, pp. 1-5.
[29] C. A. Balanis, Antenna Theory: Analysis and Design. Hoboken, NJ, USA: Wiley, 1997.
[30] N. Engheta and R. Ziolkowski, eds., Electromagnetic Metamaterials: Physics and Engineering Explorations. New York: Wiley-IEEE Press, 2006.
[31] D. R. Smith, O. Yurduseven, L. P. Mancera, and P. Bowen, “Analysis of a waveguide-fed metasurface antenna,” Physical Review Applied, 8, 2017, pp. pp. 05404-81 – 054048-16.
[32] John David Jackson, Classical Electrodynamics, 3rd ed. (Wiley, New York, 1999).
[33] Y. Liu, H. Wang, W. Zhao, M. Zhang, H. Qin, Y. Xie, “Flexible, stretchable sensors for wearable health monitoring: Sensing mechanisms, materials, fabrication strategies and features,” Sensors, vol. 18, issue 645, 2018, pp.1-35.
[34] E. Gjonaj, M. Bartsch, M. Clemens, S. Schupp, and T. Weiland, “High resolution human anatomy models for advanced electromagnetic field computations,” IEEE Trans. Magn., vol. 38, no. 2, Mar. 2002, pp. 357–360.
[35] Federal Communications Commission, “Specific absorption rate (SAR) for cellular telephones.” https://www.fcc.gov/general/specific-absorption-rate-sar-cellular-telephones#:~:text=The%20FCC%20limit%20for%20public,(1.6%20W%2Fkg).
[36] A. Altaf et al., “Isolation improvement in UWB-MIMO antenna system using slotted stub,” Electronics, vol.9, no.1582, 2020, pp.1-13.
[37] A. Y. I. Ashyap, Z. Zainal Abidin, S. H. Dahlan, H. A. Majid, M. R. Kamarudin, A. Alomainy, R. A. Abd-Alhameed, J. S. Kosha, and J. M. Noras, ‘‘Highly efficient wearable CPW antenna enabled by EBGFSS structure for medical body area network applications,’’ IEEE Access, vol. 6, 2018, pp. 77529–77541.
[38] G.-P. Gao, B. Hu, S.-F. Wang, and C. Yang, ‘‘Wearable circular ring slot antenna with EBG structure for wireless body area network,’’ IEEE Antennas Wireless Propag. Lett., vol. 17, no. 3, Mar. 2018, pp. 434–437.
[39] A. Alemaryeen and S. Noghanian, ‘‘On-body low-profile textile antenna with artificial magnetic conductor,’’ IEEE Trans. Antennas Propag., vol. 67, no. 6, Jun. 2019, pp. 3649–3656.
[40] A. Arif, M. Zubair, M. Ali, M. U. Khan, and M. Q. Mehmood, ‘‘A compact, low-profile fractal antenna for wearable on-body WBAN applications,’’ IEEE Antennas Wireless Propag. Lett., vol. 18, no. 5, May 2019, pp. 981–985.
[41] C. Mohan and S. E. Florence, ‘‘Miniaturised triangular microstrip antenna with metamaterial for wireless sensor node applications,’’ IETE J. Res., pp. 1–6, Jul. 2019.
[42] Y. J. Li, Z. Y. Lu, and L. S. Yang, ‘‘CPW-fed slot antenna for medical wearable applications,’’ IEEE Access, vol. 7, pp. 42107–42112, 2019.
[43] S. Zhu and R. Langley, ‘‘Dual-band wearable textile antenna on an EBG substrate,’’ IEEE Trans. Antennas Propag., vol. 57, no. 4, pp. 926–935, Apr. 2009.
[44] S. Velan, E. F. Sundarsingh, M. Kanagasabai, A. K. Sarma, C. Raviteja, R. Sivasamy, and J. K. Pakkathillam, ‘‘Dual-band EBG integrated monopole antenna deploying fractal geometry for wearable applications,’’ IEEE Antennas Wireless Propag. Lett., vol. 14, pp. 249–252, 2015.
[45] X.-Q. Zhu, Y.-X. Guo, and W. Wu, ‘‘A compact dual-band antenna for wireless body-area network applications,’’ IEEE Antennas Wireless Propag. Lett., vol. 15, pp. 98–101, 2016.
[46] S. Agneessens and H. Rogier, ‘‘Compact half diamond dual-band textile HMSIW on-body antenna,’’ IEEE Trans. Antennas Propag., vol. 62, no. 5, pp. 2374–2381, May 2014.
[47] S. Agneessens, S. Lemey, T. Vervust, and H. Rogier, ‘‘Wearable, small, and robust: The circular quarter-mode textile antenna,’’ IEEE Antennas Wireless Propag. Lett., vol. 14, pp. 1482–1485, 2015.
[48] K. Kamardin, M. K. A. Rahim, P. S. Hall, N. A. Samsuri, T. A. Latef, and M. H. Ullah, ‘‘Planar textile antennas with artificial magnetic conductor for body-centric communications,’’ Appl. Phys. A, Mater. Sci. Process., vol. 122, no. 4, p. 363, 2016.
[49] Z. H. Jiang, Z. Cui, T. Yue, Y. Zhu, and D. H. Werner, ‘‘Compact, highly efficient, and fully flexible circularly polarized antenna enabled by silver nanowires for wireless body-area networks,’’ IEEE Trans. Biomed. Circuits Syst., vol. 11, no. 4, pp. 920–932, Aug. 2017.
[50] H. R. Raa, A. I. Abbosh, H. M. Al-Rizzo, and D. G. Rucker, ‘‘Flexible and compact AMC based antenna for telemedicine applications,’’ IEEE Trans. Antennas Propag., vol. 61, no. 2, pp. 524–531, Feb. 2013.
[51] M. Wang et al., ‘‘Investigation of SAR reduction using flexible antenna with metamaterial structure in wireless body area network,’’ IEEE Trans. Antennas Propag., vol. 66, no. 6, pp. 3076–3086, Jun. 2018.
[52] M. A. B. Abbasi, S. S. Nikolaou, M. A. Antoniades, M. N. Stevanovi¢, and P. Vryonides, ‘‘Compact EBG-backed planar monopole for BAN wearable applications,’’ IEEE Trans. Antennas Propag., vol. 65, no. 2, pp. 453–463, Feb. 2017.
[53] Z. H. Jiang, D. E. Brocker, P. E. Sieber, and D. H. Werner, ‘‘A compact, low-profile metasurface-enabled antenna for wearable medical body area network devices,’’ IEEE Trans. Antennas Propag., vol. 62, no. 8, pp. 4021–4030, Aug. 2014.
[54] S. Yan, P. J. Soh, and G. A. E. Vandenbosch, ‘‘Low-profile dual-band textile antenna with artificial magnetic conductor plane,’’ IEEE Trans. Antennas Propag., vol. 62, no. 12, pp. 6487–6490, Dec. 2014.
[55] M. Manteghi and Y. Rahmat-Samii, “Multiport characteristics of a wide-band cavity backed annular patch antenna for multipolarization operations,” IEEE Trans. Antennas Propag., vol. 53, pp. 466–474, Jan. 2005.

Ayman A. Althuwayb received the B.Sc. degree (Hons.) in electrical engineering (electronics and communications) from Jouf University, Saudi Arabia, the M. Sc. Degree in electrical engineering from California State University, Fullerton, CA, USA, in 2015, and the Ph.D. degree in electrical engineering from Southern Methodist University, Dallas, TX, USA, in 2018. He is currently an Assistant Professor with the department of electrical engineering at Jouf University, Kingdom of Saudi Arabia. His current research interests include antenna design and propagation, microwaves and millimeter-waves, wireless power transfer, ultra-wideband and multiband antenna, filters and others.

MOHAMMAD ALIBAKHSHIKENARI (Member, IEEE) was born in Mazandaran, Iran, in February 1988. He received the Ph.D. degree (Hons.) with European Label in electronics engineering from the University of Rome ''Tor Vergata'', Italy, in February 2020. He was a Ph.D. Visiting Researcher at the Chalmers University of Technology, Sweden, in 2018. His training during the Ph.D. included a research stage in the Swedish company Gap Waves AB. He is currently with the Department of Signal Theory and Communications, Universidad Carlos III de Madrid (uc3m), Spain, as the Principal Investigator of the CONEX (CONnecting EXcellence)-Plus Talent Training Program and Marie Skłodowska-Curie Actions. He was also a Lecturer of the electromagnetic fields and electromagnetic laboratory with the Department of Signal Theory and Communications for academic year 2021–2022 and he received the ''Teaching Excellent Acknowledgement'' Certificate for the course of electromagnetic fields from Vice-Rector of studies of uc3m. Now he is spending an industrial research period in SARAS Technology Limited Company, located in Leeds, United Kingdom, which is defined as his secondment plan by CONEX-Plus Program and Marie Skłodowska-Curie Actions. His research interests include electromagnetic systems, antennas and wave-propagations, metamaterials and metasurfaces, synthetic aperture radars (SAR), multiple input multiple output (MIMO) systems, RFID tag antennas, substrate integrated waveguides (SIWs), impedance matching circuits, microwave components, millimeter-waves and terahertz integrated circuits, gap waveguide technology, beamforming matrix, and reconfigurable intelligent surfaces (RIS). He was a recipient of the three years research grant funded by Universidad Carlos III de Madrid and the European Union's Horizon 2020 Research and Innovation Program under the Marie Skłodowska-Curie Grant started in July 2021, the two years research grant funded by the University of Rome ''Tor Vergata'' started in November 2019, the three years Ph.D. Scholarship funded by the University of Rome ''Tor Vergata'' started in November 2016, and the two Young Engineer Awards of the 47th and 48th European Microwave Conference were held in Nuremberg, Germany, in 2017, and in Madrid, Spain, in 2018, respectively. His research article entitled ''High-Gain Metasurface in Polyimide On-Chip Antenna Based on CRLH-TL for Sub Terahertz Integrated Circuits'' published in Scientific Reports was awarded as the Best Month Paper at the University of Bradford, U.K., in April 2020. He is serving as an Associate Editor for (i) *Radio Science*, and (ii) *IET Journal of Engineering*. He also acts as a referee in several highly reputed journals and international conferences.

BAL S. VIRDEE graduated with a B.Sc. (Eng.) from the University of Leeds, U.K., and Ph.D. degree from the University of London, U.K. Since graduation he has worked in industry for various high-tech companies including Philips, as a research and development engineer, and at Teledyne Defence & Space as a future products developer in RF/microwave communications. He has taught in several academic institutions in the U.K. He is currently a senior professor of communications technology and director of center for communications technology at the school of computing and digital media, London Metropolitan University. He has supervised and examined numerous PhD students and has published extensively research papers at international conferences and peer-reviewed journals. His research, in collaboration with industry and academia, is in next generation wireless communications systems. He is Chair and Executive Member of the Institution of Engineering and Technology's (IET) technical and professional network committee on RF/microwave-technology. He is a charted engineer (CEng), Fellow of the IET and Senior Member of IEEE.

Nasr Rashid was born in Egypt, in 1973. He received the B.Sc. (with highest honors), M.Sc, and PhD in Electronics and Communication Engineering from Al-Azhar University, Cairo, Egypt in 1996, 2004, and 2009 respectively. He is currently an Assistant Professor in the Department of Electrical Engineering, College of Engineering, Jouf University, Sakaka, Saudi Arabia. His current research interests are in wireless communications, antennas and wave-propagations, control engineering, and signal processing.

Khaled Kaaniche was born in Tunisia in 1976. He received the BSc degree in Electrical Engineering from University of Sfax, Tunisia in 2000. In 2001, he received MSc degree in Control from INSA Lyon, France and in 2005 the Ph.D. degree in Control from UPJV France. He joined the University of Sousse, Tunisia in 2006 as an Assistant Professor in the College of Engineering. Between 2010 and 2014 he was the head of the Computer Engineering Department. His main areas of research interest are Visual Servo, Robotics, Optimization and Computer Vision. He is currently an assistant professor in the Electrical Engineering Department at Jouf University, Saudi Arabia.

Ahmed Ben Atitallah is currently an Associate Professor in Electronics at College of Engineering, Jouf University, Kingdom of Saudi Arabia. He received his PhD degree in Electronics from the University of Bordeaux1 in 2007, France and the diploma of engineer and MS degree in Electronics from the University of Sfax in 2002 and 2003, respectively, Tunisia. From 2008 to 2018, he held the position of assistant professor then associate professor in Electronics at the University of Sfax, Tunisia. His main research activities are focused on image and video processing, Algorithm-Architecture Matching, Hardware/Software Codesign, SoC/SoPC architecture, Design space exploration, Parallel architecture, Reconfigurable computing.

Ammar Armghan was born in Faisalabad, Pakistan, in February 1984. He received B.S. degree in Electrical Engineering from COMSATS University in 2006 and M.S. degree in Electronics and Communication Engineering from University of Nottingham in 2010. In 2006, he joined School of Electrical Engineering, The University of Faisalabad, as a Lecturer. In 2016, he received a Ph.D. degree from the Wuhan National lab of optoelectronic, Huazhong University of Science and Technology, Wuhan, China. He is currently working as an Assistant Professor. His research interest includes complementary metamaterial based microwave and terahertz devices.

Osama I. Elhamrawy was born in Egypt, in 1976. He received the B.S., M.S, and PhD in Electronics and Communication Engineering from Al-Azhar University, Cairo, Egypt in 1999, 2006, and 2011 respectively. He is currently an Assistant Professor in the Department of Electrical Engineering, College of Engineering, Jouf University, Sakaka, Saudi Arabia. His current research interests are in Electronics, Multilevel Inverters, and Wireless Communications.

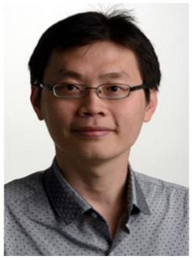

Chan Hwang See (M'14, SM'15) received a first class B.Eng. Honours degree in Electronic, Telecommunication and Computer Engineering and a Ph.D. degree from the University of Bradford, UK in 2002 and 2007, respectively. He is an associate Professor in School of Computing, Engineering and the Built Environment, Edinburgh Napier University, UK. Previously, he was Head of Electrical Engineering and Mathematics. Prior to this, he was a Senior Lecturer (Programme Leader) in Electrical & Electronic Engineering, School of Engineering, University of Bolton, UK. Before this, he was a Senior Research Fellow in the Antennas and Applied Electromagnetics Research Group within the University of Bradford. His research interests cover wireless sensor network system design, computational electromagnetism, antennas, microwave circuits, Wireless Power Transfer and acoustic sensor design. He has published over 130 peer-reviewed journal articles in these research areas. He is a co-author for one book and three book chapters. He was a recipient of two Young Scientist Awards from the International Union of Radio Science (URSI) and Asia-Pacific Radio Science Conference (AP-RASC) in 2008 and 2010, respectively. He was awarded a certificate of excellence for his successful Knowledge Transfer Partnership (KTP) with Yorkshire Water on the design and implementation of a wireless sensor system for sewerage infrastructure monitoring in 2009. Dr. See is a Chartered Engineer, Fellow of the Institution of Engineering and Technology. He is also a Fellow of the Higher Education Academy, a full member of the EPSRC Review College, an Associate Editor for IEEE Access and an Editor for Journal of Electronics and Electrical Engineering, Scientific Reports, PeerJ Computer Science, PLOS One and Wireless Power Transfer Journals.

FRANCISCO FALCONE (M'05, SM'09) received the degree in telecommunication engineering and the Ph.D. degree in communication engineering from the Universidad Pública de Navarra (UPNA), Spain, in 1999 and 2005, respectivelyFrom 1999 to 2000, he was Microwave Network Engineer, Siemens-Italtel, Málaga. From 2000 to 2008, he was Mobile Access Network Engineer, Telefónica Móviles, in Pamplona. In 2009 he co-founded Tafco Metawireless, spin-off of the UPNA (with EIBT national label), of which he was its first manager. In parallel, from 2003 to 2009 he was Assistant Lecturer in the Department of Electrical and Electronic Engineering, UPNA. In June 2009 he became Associate Professor and since September 2022, Full Professor at the EEC Dept at UPNA. From 2011 to 2012 he was secretary of the Department of Electrical, Electronic and Communication Engineering of UPNA. From January 2012 to July 2018 and from July 2019 to November 2021 he was Head of the Department of Electrical, Electronic and Communication Engineering of the UPNA. In 2018 he was Visiting Professor at Kuwait College of Science and Technology, Kuwait, for three months. He is also affiliated with the Smart Cities Institute of the Public University of Navarra, a multidisciplinary research institute with over 100 researchers, being Head of the Institute since May 2021, working on contextual and interactive environments solutions, through the integration of heterogeneous wireless communications networks, based on HetNet and IoT. Since June 2022, he is Distinguished Visiting Professor in Telecommunications School of Engineering and Science, Tecnologico de Monterrey, Mexico. His research interests are related to computational electromagnetics applied to the analysis of complex electromagnetic scenarios, with a focus on the analysis, design, and implementation of heterogeneous wireless networks to enable context-aware environments. He has over 600 contributions in indexed international journals, book chapters, and conference contributions. He has been awarded several research awards: CST Best Paper Award 2003 and 2005, Prize of the Official Association of Telecommunications Engineers 2005 for the Best Doctoral Thesis, UPNA PhD Award 2004-2006 in Experimental Sciences, 1st Prize Juan López de Peñalver 2010 to the best young researcher, Real Academia de Ingeniería de España, XII Talgo Foundation Award for Technological Innovation with the proposal "Implementation of an Environment for the Railway Ecosystem", ECSA-2 Best Paper Award (2015), Best Paper Award IISA (2015), ECSA Award -3 Best Paper Award (2016), ECSA-4 Best Paper Award (2018), Best Paper Award ISSI (2019) and IIoT 2020 Best Paper Award.